Fast-ion-beam laser and laser-rf double-resonance measurements of hyperfine structure in ^{83}Kr II

T. J. Scholl, T. D. Gaily, R. A. Holt, and S. D. Rosner
The University of Western Ontario, London, Ontario, Canada N6A 3K7
(Received 30 September 1985)

We have applied the methods of fast-ion-beam laser spectroscopy (FIBLAS) and laser-rf double resonance to study the $4p^4(^3P)4d\,^4D_{7/2} \rightarrow 4p^4(^3P)5p\,^4D^o_{7/2}$ transition at 642.018 nm in ^{83}Kr II. The effective hyperfine constants of the $4d\,^4D_{7/2}$ state were measured by radiofrequency magnetic resonance, with the results (in MHz) $A=-43.5132(3)$, $B=-294.921(5)$, and $C=-0.0030(6)$. The FIBLAS results for the $5p\,^4D^o_{7/2}$ effective hyperfine constants are (in MHz) $A'=-145.29(7)$ and $B'=536(2)$.

I. INTRODUCTION

The spectrum of the singly ionized krypton atom Kr II has been under investigation for many years.[1–4] In recent times, the significant role played by Kr II in gas laser physics has motivated numerous experimental studies, notably measurements of transition probabilities.[5] A relatively small number of theoretical investigations have been reported, for the most part intermediate-coupling multiconfiguration calculations.[6,7] Measurements of magnetic-dipole hyperfine interactions can be useful as a direct test of the accuracy of computed wave functions, since the nuclear dipole moment is known independently from NMR studies.[8] In the case of the electric quadrupoles and higher terms, measurements of hyperfine effects are the only method of determining nuclear properties, and accurate wave functions are needed to compute the corresponding atomic properties. In the present paper we report the first observation of hyperfine splitting in Kr II, together with very high resolution measurements of the $4p^4(^3P)4d\,^4D_{7/2}$ and $4p^4(^3P)5p\,^4D^o_{7/2}$ hyperfine intervals by the methods of fast-ion-beam laser spectroscopy (FIBLAS) and laser-rf double-resonance spectroscopy.

The FIBLAS method, first demonstrated by Andrä,[9] has been applied to a wide variety of ionic species.[10] Especially when collinear geometry is employed, this technique offers the advantage of greatly increased spectral resolution as a result of kinematic compression.[11,12] Additionally, a very high degree of selectivity is provided by the combination of mass selection and narrow-band laser excitation. The use of laser-induced fluorescence gives high detection efficiencies.

The first demonstration of laser-rf double-resonance spectroscopy of ion beams was a measurement of the hyperfine structure of the $5d\,^4D_{7/2}$ metastable state of ^{129}Xe II and ^{131}Xe II performed in 1977 by Rosner *et al.*[13] Since then only a small number of experiments[14–16] have exploited this technique, which offers linewidths limited only by the transit time of the ions through the region in which radio-frequency transitions take place.

II. EXPERIMENTAL PROCEDURE

A schematic diagram of the apparatus is shown in Fig. 1. Ions are produced in a Colutron ion source, accelerated to 3000–5000 eV, focused by an einzel lens, and mass analyzed by a Wien filter. Typical ion currents detected at the far end of the apparatus are 100–400 nA. The Wien filter has a calculated resolving power of 200 in the absence of space-charge effects. In practice, however, we are not able to achieve a clean separation of the Kr isotopes. The even-isotope peaks of krypton (with atomic masses of 80, 82, 84, and 86) are easily resolved by laser spectroscopy because their differing velocities give rise to quite different Doppler shifts; however, these peaks greatly overlap the rather extended hyperfine structure of ^{83}Kr II (nuclear spin $I=\frac{9}{2}$), complicating the optical spectrum.

The Spectra Physics 580A cw single-mode standing-wave dye laser is pumped by a Spectra Physics 165 cw argon-ion laser. A 50 wt.%–50 wt.% mixture of Rho-

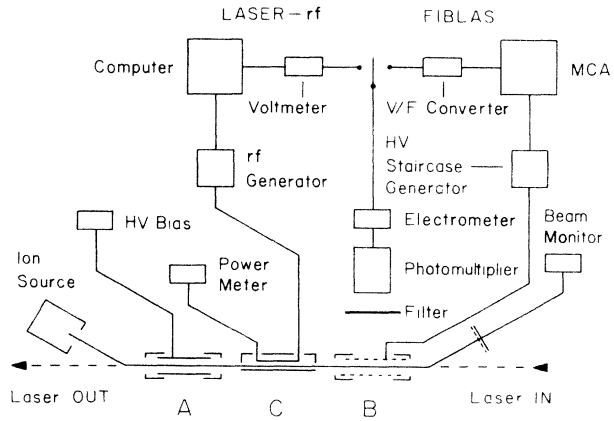

FIG. 1. Schematic diagram of the apparatus, showing the experimental configurations for both FIBLAS and laser-rf double-resonance spectroscopy.

 ©1986 The American Physical Society

damine 640 and Rhodamine 590 dissolved in ethylene glycol provides approximately 20 mW of tunable single-mode light at 642 nm. The laser frequency is locked to an iodine absorption line as an absolute frequency reference using a dc ratio method. The linearly polarized light is expanded and collimated before it enters the ion beam apparatus through a quartz Brewster window. A set of apertures limits the laser beam to a 0.48 cm diameter to reduce scattered light within the apparatus.

The ion beam is made collinear and physically overlaps with the laser beam over a total distance of ~ 90 cm. The laser wavelength is chosen so that optical resonance cannot take place when the ion beam is at ground potential. For FIBLAS measurements, the A region is used simply as an additional einzel lens, operating at a potential which ensures that the ions are not in resonance with the light. No rf power is applied to the C region, which is maintained at ground potential. The laser and ion beams interact only in the B region, in which a staircase voltage applied to a cylindrical electrode is used to Doppler scan the ions through resonance with the laser wavelength. The ions are excited by 642.018 nm light from the $4d\,^4D_{7/2}$ metastable level to the $5p\,^4D^o_{7/2}$ level and decay predominantly to the $5s\,^4P_{5/2}$ state by spontaneous emission at 435.547 nm. The laser-induced fluorescence emerging from gridded apertures in the B electrode is detected by a cooled photomultiplier which is shielded from scattered laser light by color filters. The fluorescence signal from the photomultiplier is digitized and recorded on a multichannel analyzer (MCA), which also provides the staircase scanning voltage via a 16-bit (binary digit) digital-to-analog converter (DAC) and a high-voltage operational amplifier. A typical Doppler-tuned optical spectrum taken with an ion energy of 3500 eV is shown in Fig. 2; the overlapping of even-isotope peaks with the extended hfs of ^{83}Kr II is clearly evident. The corresponding level structures of the upper and lower states, together with the observed optical transitions, are given in Fig. 3.

The laser-rf double-resonance measurements require that a population difference between adjacent hyperfine levels be created in the A region. This is achieved by applying a fixed potential to a cylindrical electrode to Doppler shift the laser wavelength into resonance with a single hyperfine component of the $4d\,^4D_{7/2} \rightarrow 5p\,^4D^o_{7/2}$ transition; the strong branching ratio for the $5p\,^4D^o_{7/2} \rightarrow 5s\,^4P_{5/2}$ decay ensures that the population of one hyperfine level of the $4d\,^4D_{7/2}$ state can be substantially depleted by the laser-induced fluorescence process. The optical pumping affects only a single hyperfine level because the linewidth of the optical resonance, due to the velocity spread of the ion beam, is ~ 50 MHz. Between the A and B regions, the ions pass through the C region where an rf magnetic field drives magnetic dipole hyperfine transitions ($\Delta F = \pm 1$) in the metastable level. If the axis of quantization is chosen along the linear polarization direction of the laser light, which is parallel to the rf magnetic field, then the selection rule is $\Delta M_F = 0$ (π polarization).

The rf magnetic field in the C region is produced by a transmission line terminated in its characteristic impedance of 50 Ω, thus presenting a constant load to the rf amplifier as the frequency is changed. Using a transmission line also ensures a uniform magnetic field amplitude over the entire 21-cm-long C region. A stripline geometry

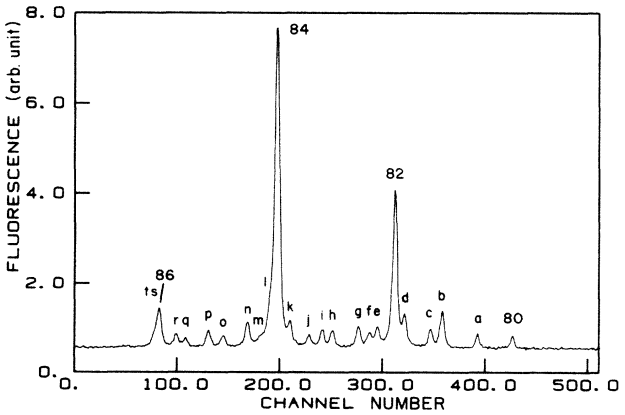

FIG. 2. Typical FIBLAS spectrum. Even-isotope peaks are labeled by their mass number. The ^{83}Kr II hyperfine components are labeled a, b, c, etc. Corresponding transitions may be found in Fig. 3.

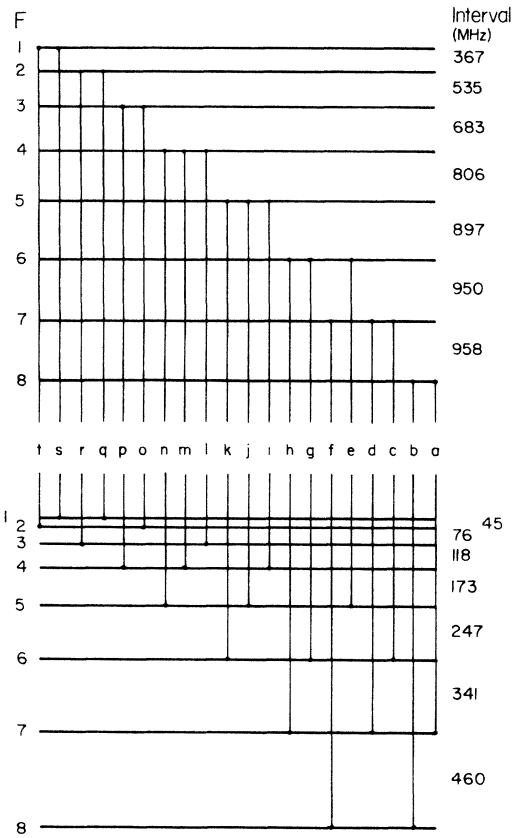

FIG. 3. Energy-level diagram of the $5p\,^4D^o_{7/2}$ and $4d\,^4D_{7/2}$ states of ^{83}Kr II showing the hyperfine structure. The transitions labeled a, b, c, etc., refer to the observed peaks in the optical spectrum (see Fig. 2).

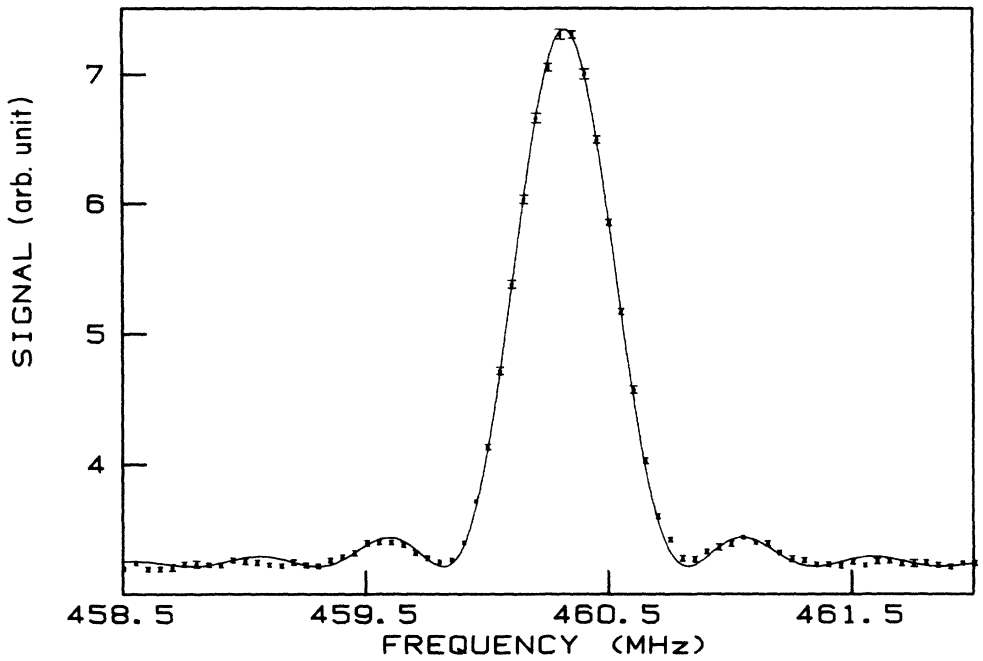

FIG. 4. Typical laser-rf double resonance spectrum. The error bars represent one standard deviation of the mean of 12 measurements taken for each point. The solid curve represents the least-squares fit of a Rabi two-level model to the data.

was chosen, with a ~1.3-cm diam cylindrical inner conductor centered between ground planes spaced ~2.2 cm apart, to maximize the field amplitude applied to the ion beam. The rf is generated by a Hewlett Packard 8660C frequency synthesizer and amplified by either a Microwave Power Devices LAB-3-110-6F amplifier or an ENI 411LA amplifier, depending upon the frequency. The synthesizer is externally programmable by a microcomputer through a parallel interface. The magnetic field of the earth is canceled by three sets of Helmholtz coils to prevent Zeeman splitting or broadening of the signal.

For the laser-rf double-resonance measurements, the fluorescence signal is digitized by a DMM and transferred through an IEEE bus to a microcomputer. Simultaneous observation of this signal on an electrometer allows the maximization of the content of the mass-83 isotope in the ion beam and determination of the Doppler-tuning voltage of a given hyperfine component. Preliminary rf signals are obtained by scanning the frequency manually over the hyperfine resonance giving an approximate frequency of the resonance and an idea of the optimum rf power. The optimum ranged from ~0.5 W for $F=1\leftrightarrow F=2$ to ~7 W for $F=7\leftrightarrow F=8$. A spectrum is recorded as the frequency is stepped across the signal in both directions to reduce systematic error from slow drifts. A pair of rf spectra is taken for each hyperfine transition, one for each direction of propagation of the rf relative to that of the ion beam. This enables us to eliminate the first-order Doppler shift (the second-order shift is negligible compared to our experimental uncertainties at these velocities). A typical rf spectrum is shown in Fig. 4. The 500-kHz linewidths are a result of the finite transit time of the ions through the C region.

TABLE I. Comparison of observed and fitted values of the hyperfine intervals in the $4d\,^4D_{7/2}$ level of Kr II. The fitted values were calculated using the hfs constants in Table II.

Transition $F\leftrightarrow F+1$	Observed frequency (MHz)	Fitted frequency (MHz)	Difference (MHz)
1↔2	44.900(2)	44.901	−0.001
2↔3	76.128(4)	76.126	0.002
3↔4	117.880(4)	117.881	−0.001
4↔5	173.678(4)	173.677	0.001
5↔6	247.034(4)	247.030	0.004
6↔7	341.450(3)	341.453	−0.003
7↔8	460.466(1)	460.466	0.000

III. ANALYSIS AND RESULTS

A least-squares fitting routine using a Rabi two-level model[17] was used to fit the laser-rf double-resonance curves for the $4d\,^4D_{7/2}$ metastable level. Theoretically, the signal is the sum of two-level models with different

TABLE II. Effective hyperfine constants (in MHz) of the $4d\,^4D_{7/2}$ level of Kr II. The constants are defined in the Appendix. The errors represent one standard deviation.

$A=$ −43.5132(3)	$A_1=$ −685.333(5)
$B=$ −294.921(5)	$A_2=$ −73.730(1)
$C=$ −0.0030(6)	$A_3=$ −0.0030(6)

TABLE III. Effective hyperfine constants (in MHz) of the $5p\,^4D^o_{7/2}$ level of Kr II. The constants are defined in the Appendix. The errors represent one standard deviation.

$A' = -145.29(7)$	$A'_1 = -2288(1)$
$B' = 536(2)$	$A'_2 = 134.0(5)$

Rabi flopping frequencies, one for each M_F value. As can be seen in Fig. 4, the fit with a simple two-level model was entirely adequate to extract the line center from the data. The fitting procedure involved fitting four parameters (the central frequency, peak amplitude, Rabi flopping frequency, and a flat background) to each resonance peak. The fitted central frequencies from pairs of spectra utilizing both directions of propagation for the rf were then averaged. The results of these fits are shown in Table I. With a total electronic angular momentum of $\frac{7}{2}$, which is smaller than the nuclear spin of $\frac{9}{2}$, there are in principle seven independent hyperfine constants.[18] A summary of the general expansion of the hyperfine interaction in terms of magnetic and electric multipoles is given for reference in the Appendix. We began our data analysis by including only the magnetic dipole and electric quadrupole terms; this gave a χ^2 per degree of freedom of 5.9. The addition of a magnetic octupole constant, which was determined to 20%, lowered the χ^2 per degree of freedom to 0.7. The fitted hyperfine intervals are listed in Table I and the hyperfine constants are given in Table II. The three hyperfine constants predict the observed lower-state hyperfine structure to within experimental error, precluding the addition of higher-order constants at our present level of accuracy. These *effective* constants have not been "corrected" for second-order effects of the hyperfine interaction. The $4p^4(^3P)4d\,^4D_{5/2}$ level from the same fine-structure multiplet is only 217 cm^{-1} away and would be expected to make significant contributions at our level of accuracy.

One possible source of systematic error in collinear geometry is the light shift of the resonant frequency due to virtual optical transitions within the C region. This has recently been observed by Borghs *et al.*[19] in Ba II. In the present experiment, the detuning of the laser light in the C region was always at least 5000 MHz. The corresponding shift of the rf resonance frequency at our light intensities is less than 1 kHz.

With the lower-state hyperfine constants determined by rf spectroscopy, the optical spectra were used to obtain the values of the $5p\,^4D^o_{7/2}$ upper-state constants. The contamination of the data by the large even-isotope peaks presents a possible source of systematic error. Of the 22 possible hyperfine lines, 20 were observed. Some of these lines are partly or totally obscured by the even-isotope

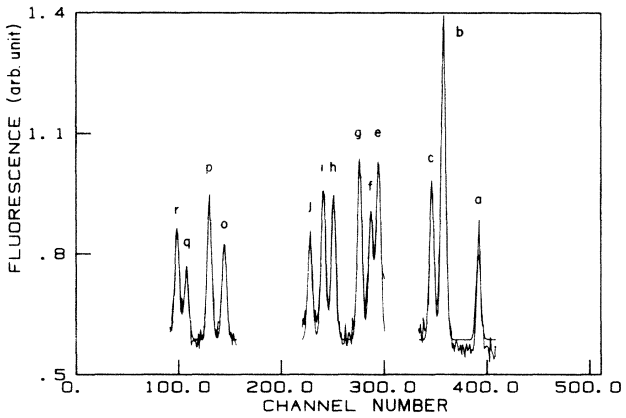

FIG. 5. A least-squares fit to the optical spectrum shown in Fig. 2 ignoring the data regions influenced by the even-isotope peaks. The fit has been plotted over the data and appears as the smooth curve.

peaks. These saturated peaks are not adequately modeled by a simple Gaussian curve, especially in the extended skirts which distort the shapes of adjacent hyperfine peaks. This problem was overcome by excluding the regions of data influenced by the even-isotope peaks. Ignoring this part of the data leaves three regions of data, including 15 hyperfine peaks, to determine the constants. A least-squares fit to the same optical spectrum that is shown in Fig. 2 is graphed with an expanded vertical scale in Fig. 5. Twelve different spectra taken with different experimental conditions were analyzed, giving the average values of the upper state hyperfine constants listed in Table III.

We are not aware of any theoretical calculations of the hyperfine constants for either of the excited states of ^{83}Kr II we have studied. The $4p^5\,^2P_{3/2}$ ground-state constants have been computed by Fraga *et al.*[20] using the nonrelativistic Hartree-Fock method. Since neither this state nor the two states studied in the present work have an open s shell, the contributions to the hyperfine splitting do not include a direct Fermi contact term, although there may be significant contributions from core-polarization of inner s shells. The largest contribution most likely arises from the open $4p$ shell, in view of the decrease of hyperfine energy with increasing n and l.

ACKNOWLEDGMENTS

We wish to thank the Natural Sciences and Engineering Research Council (NSERC) of Canada for financial support. One of us (T.J.S.) is grateful to NSERC for partial support.

APPENDIX

The hyperfine interaction between a nucleus of spin **I** and electrons in a state of total angular momentum **J** has the expectation value[18]

$$W_F = \sum_k^N A_k M(I,J;F;k) .$$

The M coefficients are given by

$$M(I,J;F;k)=\frac{(2I-k)!}{(2I)!}\frac{(2J-k)!}{(2J)!}\frac{(I+J-F)!(J-I+F)!(I-J+F)!}{(I+J+F+1)!}(k!)^2$$
$$\times\sum_z(-1)^{z+I+J-F}\frac{(2I+2J+1-z)!}{z!(2I-k-z)!(2J-k-z)![(I+J-F-z)!(k+F-I-J+z)!]^2},$$

where the sum extends over all integral values of z for which no factorial will have a negative argument. The explicit formulas for the first three orders of M are

$$M(I,J;F;1)=\frac{K}{2IJ},$$

$$M(I,J;F;2)=\frac{6}{(2I)(2I-1)(2J)(2J-1)}[K(K+1)-(4/3)I(I+1)J(J+1)],$$

$$M(I,J;F;3)=\frac{20}{(2I)(2I-1)(2I-2)(2J)(2J-1)(2J-2)}$$
$$\times\{K^3+4K^2+\tfrac{4}{5}K[-3I(I+1)J(J+1)+I(I+1)+J(J+1)+3]-4I(I+1)J(J+1)\},$$

in which $K=F(F+1)-I(I+1)-J(J+1)$. The hyperfine-interaction constants A_k, as defined by Schwartz,[18] are related to the commonly used constants A, B, and C by

$$A_1=IJA,\quad A_2=\tfrac{1}{4}B,\quad A_3=C.$$

[1]J. H. Abbink and H. B. Dorgelo, Z. Phys. **47**, 221 (1928).

[2]T. L. de Bruin, C. J. Humphreys, and W. F. Meggers, J. Res. Natl. Bur. Stand. **11**, 409 (1933).

[3]L. Minnhagen, H. Strihed, and B. Petersson, Ark. Fys. **39**, 471 (1969).

[4]K. Yoshino and Y. Tanaka, J. Opt. Soc. Am. **69**, 159 (1979).

[5]For a recent summary of lifetime and transition probability measurements, see L. Ward, A. Wännström, A. Arnesen, R. Hallin, and O. Vogel, Phys. Scr. **31**, 149 (1985).

[6]T. M. El Sherbini and A. A. Farrag, J. Phys. B **9**, 2797 (1976).

[7]N. Spector and S. Garpman, J. Opt. Soc. Am. **67**, 155 (1977).

[8]D. Brinkman, Phys. Lett. **27A**, 466 (1968).

[9]H. J. Andrä, in *Beam-foil Spectroscopy,* edited by I. A. Sellin and D. J. Pegg (Plenum, New York, 1976), Vol. 2, p. 835.

[10]For a review, see M. Dufay and M. L. Gaillard, in *Laser Spectroscopy III,* edited by J. L. Hall and J. L. Carlsten (Springer, Berlin, 1977), p. 231.

[11]S. L. Kaufman, Opt. Commun. **17**, 309 (1976).

[12]W. H. Wing, G. A. Ruff, W. E. Lamb, and J. J. Spezeski, Phys. Rev. Lett. **36**, 1488 (1976).

[13]S. D. Rosner, T. D. Gaily, and R. A. Holt, Phys. Rev. Lett. **40**, 851 (1978).

[14]U. Kötz, J. Kowalski, R. Neumann, S. Noehte, H. Suhr, H. Winkler, and G. zu Putlitz, J. Phys. A **300**, 25 (1981).

[15]U. Nielsen, O. Poulsen, P. Thorsen, and H. Crosswhite, Phys. Rev. Lett. **51**, 1749 (1983).

[16]M. Van Hove, G. Borghs, P. De Bisschop, and R. E. Silverans, Z. Phys. A **321**, 215 (1985).

[17]N. F. Ramsey, *Molecular Beams* (Clarendon, Oxford, 1956), Chap. V.

[18]C. Schwartz, Phys. Rev. **97**, 380 (1955).

[19]G. Borghs, P. De Bisschop, J. Odeurs, R. E. Silverans, and M. Van Hove, Phys. Rev. A **31**, 1434 (1985).

[20]S. Fraga, K. M. S. Saxena, and B. W. N. Lo, At. Data **3**, 323 (1971).